1xN plasmonic power splitters based on metal-insulator-metal waveguides

Chyong-Hua Chen* **and Kao-Sung Liao**

Department of Photonics & Institute of Electro-Optical Engineering, National Chiao Tung University,1001 Ta Hsueh Road, Hsinchu 30010, Taiwan

chyong@mail.nctu.edu.tw

Abstract: Novel plasmonic power splitters constructed from a rectangular ring resonator with direct-connected input and output waveguides are presented and numerically investigated. An analytical model and systematic approach for obtaining the appropriate design parameters are developed by designing an equivalent lumped circuit model for the transmission lines and applying it to plasmonic waveguides. This approach can dramatically reduce simulation times required for determining the desired locations of the output waveguides. Three examples are shown, the 1 × 3, 1 × 4, and 1 × 5 equal-power splitters, with the design method being easily extended to any number of output ports.

OCIS codes: (240.6680) Surface plasmons; (130.3120) Integrated optics devices; (310.2790) Guided waves; (350.4010) Microwaves.

References and links

1. E. Ozbay, "Plasmonics: merging photonics and electronics at nanoscale dimensions," Science **311**(5758), 189–193 (2006).
2. R. Zia, J. A. Schuller, A. Chandran, and M. L. Brongersma, "Plasmonics: the next chip-scale technology," Mater. Today **9**(7–8), 20–27 (2006).
3. T. W. Lee and S. Gray, "Subwavelength light bending by metal slit structures," Opt. Express **13**(24), 9652–9659 (2005).
4. G. Veronis and S. Fan, "Bends and splitters in metal-dielectric-metal subwavelength plasmonic waveguides," Appl. Phys. Lett. **87**(13), 131102 (2005).
5. R. J. Walters, R. V. A. van Loon, I. Brunets, J. Schmitz, and A. Polman, "A silicon-based electrical source of surface plasmon polaritons," Nat. Mater. **9**(1), 21–25 (2010).
6. P. Neutens, P. Van Dorpe, I. De Vlaminck, L. Lagae, and G. Borghs, "Electrical detection of confined gap plasmons in metal-insulator-metal waveguides," Nat. Photonics **3**(5), 283–286 (2009).
7. X. S. Lin and X. G. Huang, "Tooth-shaped plasmonic waveguide filters with nanometeric sizes," Opt. Lett. **33**(23), 2874–2876 (2008).
8. J. Tao, X. G. Huang, X. S. Lin, Q. Zhang, and X. Jin, "A narrow-band subwavelength plasmonic waveguide filter with asymmetrical multiple-teeth-shaped structure," Opt. Express **17**(16), 13989–13994 (2009).
9. J. Q. Liu, L. L. Wang, M. D. He, W. Q. Huang, D. Wang, B. S. Zou, and S. Wen, "A wide bandgap plasmonic Bragg reflector," Opt. Express **16**(7), 4888–4894 (2008).
10. A. Hosseini and Y. Massoud, "A low-loss metal-insulator-metal plasmonic Bragg reflector," Opt. Express **14**(23), 11318–11323 (2006).
11. S. Passinger, A. Seidel, C. Ohrt, C. Reinhardt, A. Stepanov, R. Kiyan, and B. Chichkov, "Novel efficient design of Y-splitter for surface plasmon polariton applications," Opt. Express **16**(19), 14369–14379 (2008).
12. N. Nozhat and N. Granpayeh, "Analysis of the plasmonic power splitter and MUX/DEMUX suitable for photonic integrated circuits," Opt. Commun. **284**(13), 3449–3455 (2011).
13. Z. Han and S. He, "Multimode interference effect in plasmonic subwavelength waveguides and an ultra-compact power splitter," Opt. Commun. **278**(1), 199–203 (2007).
14. Y. Guo, L. Yan, W. Pan, B. Luo, K. Wen, Z. Guo, H. Li, and X. Luo, "A plasmonic splitter based on slot cavity," Opt. Express **19**(15), 13831–13838 (2011).
15. J. Liu, H. Zhao, Y. Zhang, and S. Liu, "Resonant cavity based antireflection structures for surface plasmon waveguides," Appl. Phys. B **98**(4), 797–802 (2010).
16. P. Ginzburg and M. Orenstein, "Plasmonic transmission lines: from micro to nano scale with λ/4 impedance matching," Opt. Express **15**(11), 6762–6767 (2007).
17. S. E. Kocabas, G. Veronis, D. A. B. Miller, and S. Fan, "Transmission line and equivalent circuit models for plasmonic waveguide components," IEEE J. Sel. Top. Quantum Electron. **14**(6), 1462–1472 (2008).
18. K. Chang and L. H. Hsieh, *Microwave Ring Circuits and Related Structures* (Wiley, 2004).

#179928 - $15.00 USD Received 16 Nov 2012; revised 31 Jan 2013; accepted 4 Feb 2013; published 11 Feb 2013

19. A. D. Rakic, A. B. Djurisic, J. M. Elazar, and M. L. Majewski, "Optical properties of metallic films for vertical-cavity optoelectronic devices," Appl. Opt. **37**(22), 5271–5283 (1998).

1. Introduction

Plasmonic waveguides have potential use in enabling energy-efficient and ultrahigh-density photonic integrated circuits (PICs) and for integrating optical components into microelectronic integrated circuits (ICs) at the nanoscale level owing to the strong field confinement of the surface plasmon polaritons (SPPs) propagating along the interface between a metal and a dielectric [1, 2]. Among various plasmonic waveguides, the metal–insulator–metal (MIM) structure allows optical modes to be highly confined within the sub-wavelength insulator layer and to propagate in a sharp bend with low additional loss [3, 4]. Additionally, they are able to be easily manufactured using existing nanofabrication techniques [5, 6].

Many compact all-optical devices based on MIM plasmonic waveguides have been proposed and investigated, including filters [7, 8], Bragg reflectors [9, 10], and power splitters [4, 11–14]. Equal-power splitters are essential components to multi-way PIC systems, which distribute the input power equally to several output ports. Several schemes have been proposed, including branching-type power splitters which connect multiple two-branch structures in tandem [4, 11, 12], multimode interference (MMI) power splitters [13] and slot-cavity based power splitters [14]. The size of a cascaded coupler expands as the number of output ports increase, giving rise to a large insertion loss [12]. The relatively low transmission efficiency is observed in a MMI power splitter because of the reflections between the single mode and multimode waveguides [13]. Furthermore, although a plasmonic splitter based on a slot cavity has a compact size, a rather large transmission loss is obtained due to indirect-connected input and output waveguides [14].

In this paper, we present a new equal-power splitter consisting of a rectangular ring resonator with direct-connected input and output waveguides. We analytically establish the equivalent lumped network of the transmission lines for this structure by using microwave engineering approaches and systematically determine the locations of the output waveguides by sequentially obtaining 1:1 voltage ratios between the adjacent output waveguides. To validate the predictions from our model, plasmonic power splitters with various number of output ports are numerically demonstrated by using a two-dimensional (2D) finite difference time domain (FDTD) method.

2. Design of plasmonic power splitters

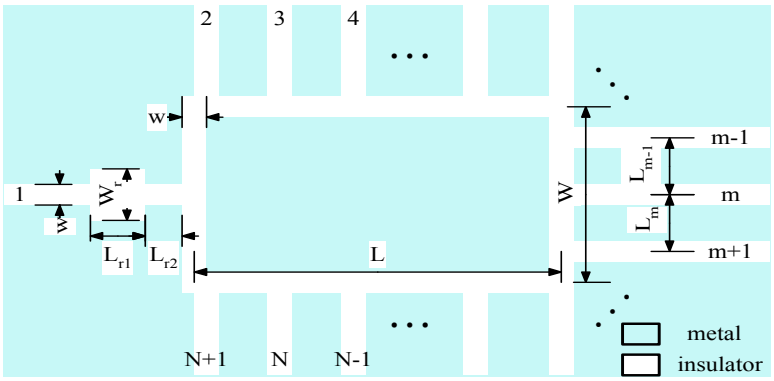

Fig. 1. Schematic diagram of the proposed power splitter

Figure 1 schematically shows the configuration of the proposed N-way power splitter where an input and N output waveguides are directly connected to a rectangular ring resonator with length L and width W. The input signal at port 1 splits among output ports 2, 3, …, and N + 1. The output ports are located symmetrically on either side of the resonator with respect to the

#179928 - $15.00 USD Received 16 Nov 2012; revised 31 Jan 2013; accepted 4 Feb 2013; published 11 Feb 2013

input port 1 to obtain identical output powers. The widths of the ring, the input waveguide and the output waveguide are all equal to w. A two-layer antireflection (AR) resonator structure is inserted between the input waveguide and the ring structure to diminish the reflection at port 1 [15]. The widths of these two layers are W_r and w, respectively. The corresponding lengths are L_{r1} and L_{r2}, respectively.

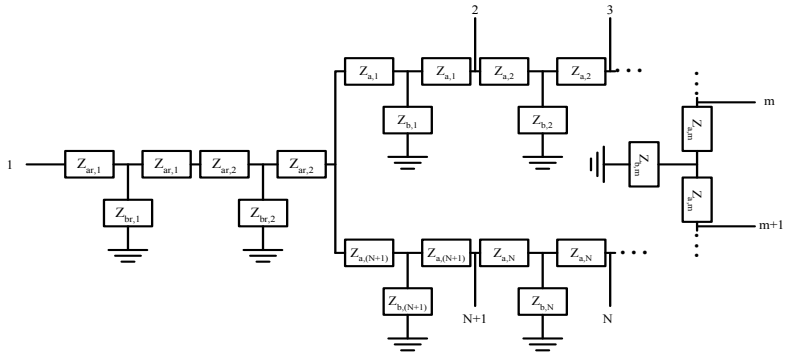

Fig. 2. Equivalent electrical circuit of the proposed structure

Here, a transverse electromagnetic (TEM) transmission line (TL) model is employed to describe the mode propagation of the MIM waveguide [16, 17]. The total equivalent circuit of this structure is illustrated in Fig. 2. The ring resonator is viewed as a closed-loop transmission line. Each waveguide segment of a ring resonator with length L_m is represented by an equivalent T-lumped circuit model with lumped parameters of $Z_{a,m}$ and $Z_{b,m}$, for m = 1, 2, …, and N + 1 [18]. These parameters are expressed as follows:

$$Z_{a,m} = jZ_o \tan\left(\beta_r L_m / 2\right) \tag{1}$$

$$Z_{b,m} = -jZ_o \csc\left(\beta_r L_m\right) \tag{2}$$

where β_r is the propagation constant of the line, and Z_o is the characteristic impedance of the transmission line, calculated by $Z_o = \dfrac{\beta_r w}{\omega \varepsilon_{in}}$ with insulator permittivity ε_{in} and frequency of incidence ω [16, 17].

It is known that the transmitted power at the m-th port can be obtained by calculating the scattering parameter $S_{m,1}$ which is proportional to the propagation voltage V_m on the transmission line of the m-th port as all the output ports are terminated in matched loads Z_o. Thus, to obtain equal power at all the output ports, the amplitude of the voltage ratio at any two output ports should be 1.

Due to the structural symmetry, i.e., $L_1 = L_{N+1}$, $L_2 = L_N$…, $V_2 = V_{N+1}$, $V_3 = V_N$…. Then, the analysis of the lumped circuit can be simplified, as shown in Fig. 3(a) and 3(b) which are the simplified circuit models looking from the port 1 with odd N and even N, respectively, without including the AR structure. Let M = N/2 for even N and M = (N + 1)/2 for odd N. We define VR(m) as the ratio of the voltage V_{m+1} to V_m which is

$$VR(m) = \frac{V_{m+1}}{V_m} = \frac{Z_{eq,m+1}}{Z_{a,m} + Z_{eq,m+1}} \frac{Z_{b,m} \| (Z_{a,m} + Z_{eq,m+1})}{Z_{a,m} + Z_{b,m} \| (Z_{a,m} + Z_{eq,m+1})}, \text{m=2, 3} \cdots \text{M} \tag{3}$$

where $Z_{eq,m+1}$ is the equivalent impedance as seen from the (m + 1)-th port, calculated by $Z_{eq,m+1} = Z_o \| \left[Z_{a,m+1} + Z_{b,m+1} \| (Z_{a,m+1} + Z_{eq,m+2}) \right]$. Two vertical lines "||" represent the total

#179928 - $15.00 USD Received 16 Nov 2012; revised 31 Jan 2013; accepted 4 Feb 2013; published 11 Feb 2013

impedance of two impedances in parallel. $Z_{eq,M+1} = 2Z_o$ for odd N, and $Z_{eq,M+1} = Z_o \,\|\left(Z_{a,M+1} + 2Z_{b,M+1}\right)$ for even N.

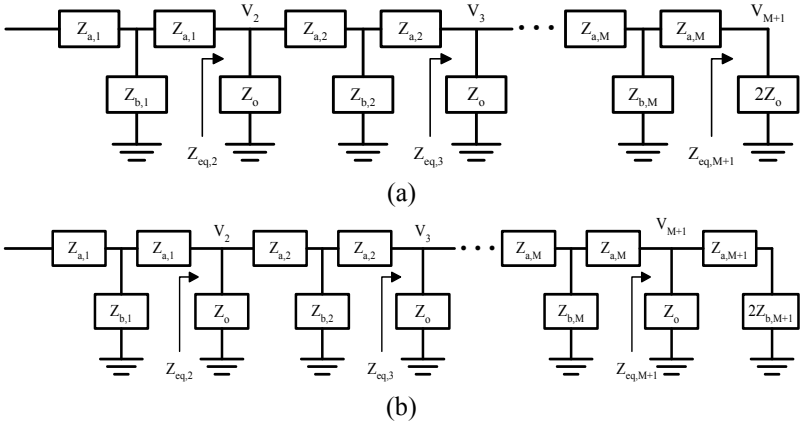

Fig. 3. Simplified circuit model of the proposed splitter for (a) odd N and (b) even N

From Eq. (3), VR(m) is independent of the line lengths of L_1, L_2, …, and L_m. Accordingly, step by step, we can achieve all amplitudes of VR equal to 1. First, we start by finding the appropriate line length of L_M to achieve the amplitude of VR(M) equal to 1, which is only a function of L_M. In the case that N is even, we can arbitrarily choose the line length of L_{M+1} to decide the value of $Z_{eq,M+1}$. Next, we determine the line length of L_{M-1} such that the amplitude of VR(M-1) is 1, which becomes a function of the single variable L_{M-1} as L_M is selected. Successively, we repeat the previous procedure recursively to find the other line lengths except for L_1.

The reflected power at port 1 can be realized by the scattering parameter S_{11} expressed as

$$S_{11} = \frac{Z_{in} - Z_o}{Z_{in} + Z_o} \tag{4}$$

where Z_{in} is the equivalent input impedance of this whole structure, which is $\left[Z_{a,1} + Z_{b,1} \,\|\, (Z_{a,1} + Z_{eq,2})\right] / 2$.

Since all the line lengths except L_1 are known, L_1 becomes the only variable of S_{11}. To diminish the reflected power at port 1, we can select the line length of L_1 to have the minimal amplitude of S_{11}. However, sometimes the minimal amplitude of S_{11} is unacceptable, and then the AR structure is applied to effectively mitigate the reflected power without changing all the values of VRs. In the following section, we numerically explore several designs to illustrate the above-mentioned design concepts.

3. Numerical results

To confirm our design analysis, here we use the example of the Ag-air-Ag waveguide with the dielectric constant of silver described by the five-term Drude-Lorentz model [19]:

$$\varepsilon(\omega) = \varepsilon_\infty - \frac{\omega_p^{\,2}}{\omega^2 + i\gamma\omega} - \sum_{n=1}^{5} \frac{\Delta\varepsilon_n \omega_n^{\,2}}{\omega^2 - \omega_n^{\,2} + i\gamma_n \omega} \tag{5}$$

where $\varepsilon_\infty = 1.0$ is the relative permittivity in the infinity frequency, $\omega_p = 1.258 \times 10^{16}$ rad/sec is the bulk plasma frequency, and $\gamma = 7.295 \times 10^{13}$ rad/sec is a damping constant. ω_n, γ_n and $\Delta\varepsilon_n$ are the oscillator resonant frequencies, the damping factors and weighting factors associated

#179928 - $15.00 USD Received 16 Nov 2012; revised 31 Jan 2013; accepted 4 Feb 2013; published 11 Feb 2013

with the Lorentzian peaks, respectively. All the parameters of this Drude - Lorentz model can be found in Ref [19].

The commercial software 2D FDTD simulator (Fullwave, RSOFT Design Inc.) is utilized to calculate the field propagation behavior and the performance of the proposed structure with w of 50 nm. The incidence is the fundamental TM mode of this MIM waveguide at the wavelength λ_0 of 1550 nm. A 50 nm perfectly matched layer (PML) boundary with reflectivity of 10^{-8} is applied. The grid sizes in the transverse direction, x, and transmission direction, z, are $\Delta x = \Delta z = 5$ nm. As the grid sizes are smaller than 5 nm, the transmission varies within ± 2%.

3.1 Odd N

First, take an example of N = 3. In this case, voltage ratio VR(2) is a function of the line length L_2. Figure 4(a) shows the amplitude of VR(2) for varying line length L_2. As we can see, the amplitude of VR(2) oscillates with a period of 550 nm, corresponding to an optical length of a half λ_0. Furthermore, the amplitude of oscillation gradually decreases because of the complex propagation constant. The amplitude of VR(2) equals 1 when L_2 equals 0, 515 nm, 588 nm, etc. Let L_2 be 515nm, then the amplitude variation of S_{11} on L_1 is illustrated in Fig. 4(b). A periodic oscillation between 0 and 1 with increasing L_1 is observed and the local minima are obtained at $L_1 = 260 + 550 \times l$ nm, with $l = 0, 1, 2\ldots$. As shown in Fig. 4(b), the minimum value is approximately 0.14, which is unsatisfactory for a power splitter. Let L and W be 295 and 1030 nm, respectively, corresponding to L_1 of 810 nm and L_2 of 515 nm. Then, the reflection at λ_0 is mitigated as W_r, L_{r1} and L_{r2} are 100, 30 and 155 nm, respectively.

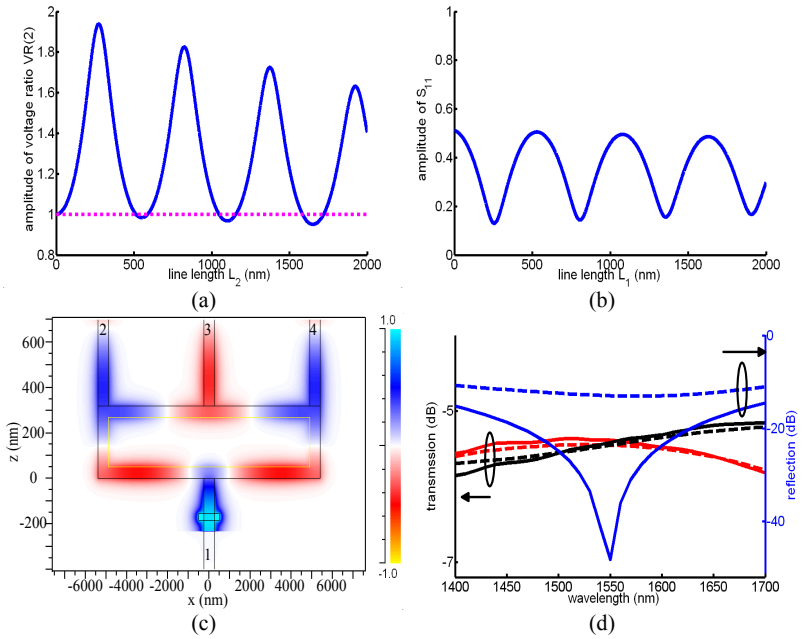

Fig. 4. (a) Variation of voltage ratio VR(2) on L_2, (b) variation of S_{11} on L_1, (c) layout of the designed 1 × 3 power splitter and the corresponding field evolution and (d) transmission and reflection spectra obtained by the FDTD method (solid lines) and by the TL model (dashed lines). The dotted magenta curve is a straight line of VR(2) = 1. The blue, red and black curves represent the calculated powers at ports 1, 2 and 3, respectively.

Figure 4(c) shows the design and the field evolution of this 1 × 3 power splitter. The transmitted powers obtained by the FDTD method are −5.41, −5.39 and −5.41 dB with respect to ports 2, 3, and 4. Notice that the powers at ports 2 and 4 are identical owing to structural symmetry. Additionally, the output powers at the ports 2 and 3 are approximately

#179928 - $15.00 USD Received 16 Nov 2012; revised 31 Jan 2013; accepted 4 Feb 2013; published 11 Feb 2013

identical. This small deviation is due to the slight inaccuracy of the TL model at λ_0. The reflected power is effectively reduced to –48.15 dB. The insertion loss of this device is –0.63 dB, mainly resulting from the transmission loss propagating through the ring and AR resonator structures. Figure 4(d) depicts the wavelength dependence of the powers at the ports 1, 2 and 3, calculated both by the TL model and by the FDTD method. As shown, the two simulated results are in close agreement. Moreover, the simulated output powers at the ports 2 and 3 are very close to each other over the broad wavelength range of 1400 to 1700 nm. On the other hand, the reflection is very wavelength selective with a steep V-shaped spectral curve. The bandwidth for reflection less than –20 dB is obtained over a wavelength range of 1460 to 1630 nm.

Next, we extend the aforementioned design to realize a 1 × 5 power splitter. We first set L_3 to be 515 nm to achieve the amplitude of VR(3) of 1. Then, we search for the line length of L_2 to obtain the amplitude of VR(2) equal to 1. Figure 5(a) shows the amplitude variation of VR(2) with L_3 of 515 nm on L_2. An oscillation with a period of 550 nm is observed, and the amplitude of VR(2) becomes 1 only as L_2 = 0 nm. Let L_2 = 0 nm and L_3 = 515 nm. The corresponding line lengths of L_1 to acquire the minimal amplitude of S_{11} are 270 + 550 × l nm, with l = 0, 1, 2…, as illustrated in Fig. 5(b). The reflection can be further minimized as W_r, L_{r1} and L_{r2} are 40, 45 and 115 nm, respectively.

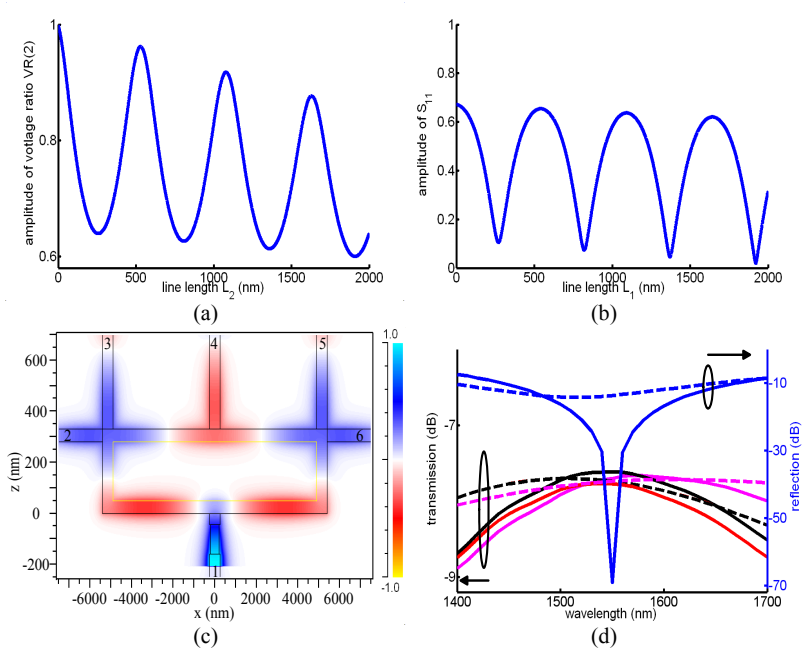

Fig. 5. (a) Variation of voltage ratio VR(2) on L_2, (b) variation of S_{11} on L_1, (c) layout of the designed 1 × 5 power splitter and the corresponding field evolution and (d) transmission and reflection spectra obtained by the FDTD method (solid lines) and by the TL model (dashed lines). The blue, red, black and magenta curves represent the calculated powers at ports 1, 2, 3 and 4, respectively.

Figure 5(c) shows the layout and its FDTD field evolution of the design with L of 1030 nm and W of 305 nm, corresponding to L_1 of 820 nm, L_2 of 0 nm and L_3 of 515 nm. The transmitted powers obtained by the FDTD method are –7.78, –7.62, –7.70, –7.62 and –7.78 dB with respect to output ports 2, 3, 4, 5 and 6. The reflected power is effectively reduced to –69.07 dB. The insertion loss of this device is –0.70 dB. Figure 5(d) depicts the power at the ports 1, 2, 3, and 4 as a function of wavelength. The performance has similar tendencies as those obtained in the aforementioned 1 × 3 power splitter except that the transmission is

#179928 - $15.00 USD Received 16 Nov 2012; revised 31 Jan 2013; accepted 4 Feb 2013; published 11 Feb 2013

smaller, roughly less by −2.3 dB. The bandwidth for reflection less than −20 dB is obtained over a wavelength range of 1520 to 1580 nm.

4.2 Even N

Here, we study the design example of a 1 × 4 power splitter. As before, we first arbitrarily choose the line length of L_3 to acquire the value of $Z_{eq,3}$. Figure 6(a) illustrates the amplitude of VR(2) as the line length L_2 is varied at L_3 = 250 nm. The amplitude of VR(2) oscillates with period of 550 nm and becomes 1 as L_2 is 0, 200 nm, 557 nm, …. Let L_2 be 200 nm, and then the amplitude variation of S_{11} on L_1 is displayed in Fig. 6(b). It shows the local minima at $L_1 = 239 + 550 \times l$ nm, l = 0, 1, 2…. Let L and W be 464 and 650 nm, respectively, corresponding to L_1 of 789 nm, L_2 of 200 nm and L_3 of 250 nm. The reflection is minimized as W_r, L_{r1} and L_{r2} are 185, 0 and 30 nm, respectively. Figure 6(c) shows the layout and the field evolution of this 1 × 4 power splitter. The transmitted powers are −6.76, −6.51, −6.51, and −6.76 dB with respect to the output ports 2, 3, 4, and 5. The reflected power is reduced to −38.89 dB. The insertion loss of this device is −0.61 dB. Figure 6(d) depicts the power at the ports 1, 2, and 3 as a function of wavelength. The calculated transmission spectra obtained by the FDTD method is shifted to shorter wavelengths by roughly 35 nm compared with those obtained by the TL model. The bandwidth for reflection less than −20 dB is obtained over a wavelength range of 1520 to 1580 nm.

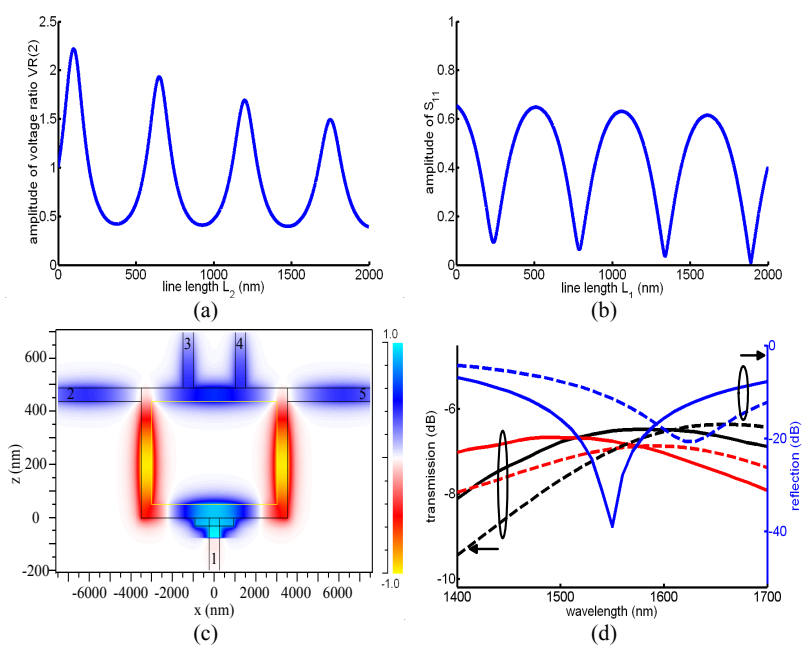

Fig. 6. (a) Variation of voltage ratio VR(2) on L_2, (b) variation of S_{11} on L_1, (c) layout of the designed 1 × 4 power splitter and the corresponding field evolution and (d) transmission and reflection spectra obtained by the FDTD method (solid lines) and by the TL model (dashed lines). The blue, red and black curves represent the calculated powers at ports 1, 2 and 3, respectively.

4. Conclusion

A new type of plasmonic power splitter is proposed and analyzed. This device consists of a rectangular ring resonator with direct-connected input and output waveguides. The theoretical structure is investigated using an equivalent circuit model and analytical expressions to obtain equal output powers at all the output ports. The appropriate line lengths are attained by

#179928 - $15.00 USD Received 16 Nov 2012; revised 31 Jan 2013; accepted 4 Feb 2013; published 11 Feb 2013

finding the solution that results in all VR amplitudes equal to 1. Three illustrative examples with different numbers of output ports are simulated by using the FDTD method to confirm our analytical model. Simulation results substantiate that this approach can effectively acquire the targeted design parameters without lengthy computation time. In addition, this structure can be easily extended to designs with a greater number of output ports. The insertion loss of this structure is primarily attributed to propagation losses in the ring resonator and the AR structure, and the bandwidth is predominantly limited by the wavelength response of the AR structure. Enhanced predictions can be achieved by including equivalent circuits for photonic T-junctions, crossings and 90° bends.

#179928 - $15.00 USD Received 16 Nov 2012; revised 31 Jan 2013; accepted 4 Feb 2013; published 11 Feb 2013